IEEE Access
Multidisciplinary | Rapid Review | Open Access Journal

Received January 31, 2020, accepted February 25, 2020, date of publication March 2, 2020, date of current version March 13, 2020.

Digital Object Identifier 10.1109/ACCESS.2020.2977382

Reference Solutions for Time Domain Electromagnetic Solvers

SOICHIRO MASUDA, SEIYA KISHIMOTO, AND SHINICHIRO OHNUKI, (Member, IEEE)
College of Science and Technology, Nihon University, Tokyo 101-8308, Japan

Corresponding author: Shinichiro Ohnuki (ohnuki.shinichiro@nihon-u.ac.jp)

This work was supported in part by the Japan Society for the Promotion of Science (JSPS) KAKENHI Grant Number JP17 K06401, and in part by the Nihon University College of Science and Technology Project for Research.

ABSTRACT In this study, a highly precise time domain solution of electromagnetic fields for a canonical structure is derived. Our reference solution is extremely useful for researchers, engineers, and developers to evaluate the accuracy of their computational results using commercial software or their self-developed codes. Rigorous solutions of a cylinder or sphere, which consists of a homogeneous medium, are derived in the complex frequency domain; they are numerically transformed into the time domain using fast inversion of Laplace transform. In addition, the field distribution at the desired specific observation time can be easily obtained. Furthermore, the numerical accuracy of the computational electromagnetic solvers is evaluated.

INDEX TERMS Reference solutions, time domain solver, fast inverse Laplace transform, finite-difference time-domain, nonlocal effects.

I. INTRODUCTION

Time domain analysis of electromagnetic fields is indispensable for various applications, such as designing computer chips, antennas, optics devices, analysis of propagation for wireless communication, and medical equipment [1]–[10]. Many commercial software packages based on time domain solvers have recently become available, which are powerful tools for industrial design and modeling. However, evaluating the reliability and accuracy of the computational results remains difficult because rigorous solutions of time domain responses are very limited [11].

A highly precise time domain solution of electromagnetic fields for a canonical structure is derived in this study. Specifically, our reference solution can obtain the field distributions for a desired specific observation time, as shown in Fig. 1. There are no limits for time step size, and it is suitable for evaluating time domain analysis methods, such as the finite-difference time-domain (FDTD) method [4], [12], [13]. The objective of this study is to propose an evaluation method for the reliability of time domain electromagnetic solver. By comparing with our obtained results at specific observation time, end users or developers can easily evaluate the accuracy of their computational results using commercial software or self-developed codes. The degree of accuracy for solving canonical problems are important for representing the accuracy of the analysis method. Our precise time domain electromagnetic responses can be obtained using the following procedure: rigorous solutions or highly accurate numerical results of electromagnetic waves are computed

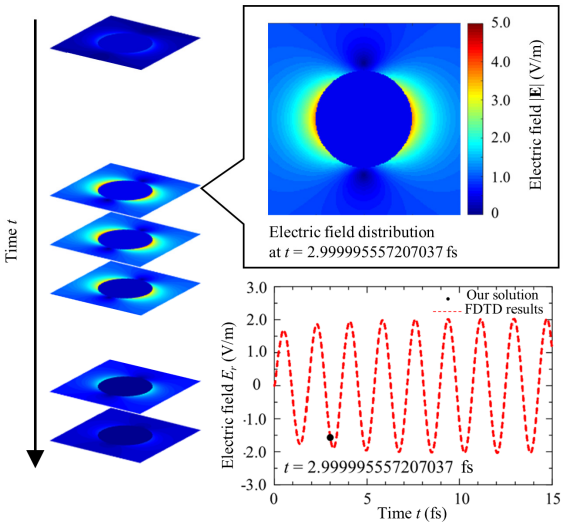

FIGURE 1. Example of our reference solution. Electromagnetic field distribution at the desired specific observation time can be obtained easily and efficiently, which is suitable for evaluating time domain solvers.

The associate editor coordinating the review of this manuscript and approving it for publication was Wei E.I. Sha.

in the complex frequency domain. The waves in the complex frequency domain are numerically transformed into time domain using fast inversion of Laplace transform (FILT) [14], [15]. The instantaneous value is easily and efficiently obtained. Furthermore, it is an error-controllable method, and the number of digits of accuracy for our reference solution can be strictly evaluated to select the approximate parameter properly.

In the formulation section, an example of electromagnetic fields in the complex frequency domain is determined and shown here. The scatterer is assumed to be a metallic nanocylinder. The hydrodynamic Drude model, which considers nonlocal effects, describes the characteristics of a metal for the wavelength light band [16], [17]. Although the problems are canonical and the shapes are limited, their solution can be obtained mathematically. Evaluation of the computational accuracy of the time domain solver, i.e., the FDTD method, is demonstrated in this study through comparison with our reference solutions. Further, the accuracy of time domain response estimated at a specific observation time is shown.

For generic purposes, the reference solutions for a perfect electric conducting cylinder, dielectric cylinder, and metallic nanosphere are derived and discussed in the appendix.

II. FORMULATION

A. FAST INVERSE LAPLACE TRANSFORM

To obtain the time domain solutions, the electromagnetic field in the complex frequency domain is transformed using FILT. In our algorithm, the sampling complex frequency can be easily decided, and the reference solution at a single moment in time is accurately obtained. To accomplish this, the exponential function in the Bromwich integral is replaced with the cosine in the hyperbolic function [14]. By substituting this approximated function into the integrand and using the residue theorem, the approximated time domain function $f_{ec}(t, \alpha)$ can be evaluated using the following equation:

$$f(t) \approx f_{ec}(t, \alpha) = \frac{e^{\alpha}}{t} \sum_{n=1}^{\infty} F_n \tag{1}$$

where

$$F_n = (-1)^n \operatorname{Im}[F(s_n)] \tag{2}$$

$$s_n = \frac{\alpha + j(n - 0.5)\pi}{t} \tag{3}$$

and $F(s)$ is the image function of the original time domain function $f(t)$. In this study, it can be obtained by analytical solution. Generally, an image function can be computed by complex frequency domain solvers. The sampling complex frequencies for the inverse Laplace transform are determined by Eq. (3). By truncating the infinite series, the final expression can be obtained as,

$$f_{ec}(t, a) = \frac{e^{\alpha}}{t} \sum_{n=1}^{k} F_n \tag{4}$$

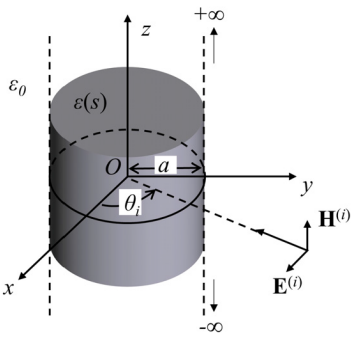

FIGURE 2. Geometry and coordinate system of the cylinder. The scatterer consists of general homogeneous media with permittivity $\varepsilon(s)$ and radius a. $\mathbf{E}^{(i)}$ and $\mathbf{H}^{(i)}$: incident waves, θ_i: angle of incidence.

where k is the truncation number. Here, the accuracy of f_{ec} can be controlled by an approximation parameter α [14], [15]. The instantaneous field distribution at an observation time t can be accurately and efficiently solved using the summation in Eq. (4).

B. ELECTROMAGNETIC FIELDS FOR A CYLINDER IN THE COMPLEX FREQUENCY DOMAIN

The scatterer is assumed to be a cylinder of radius a, and to be uniform along the z-axis and consisting of general homogeneous media with permittivity $\varepsilon(s)$, as shown in Fig. 2. Here, $\mathbf{H}^{(i)}$ and $\mathbf{E}^{(i)}$ are the incident incoming waves. The incident wave is a plane wave (in this case, the H-wave), and the magnetic field has only the z-component and is incident at angle θ_i. In this section, the time dependence is characterized by $\exp(st)$; here, s is the complex frequency given by $\sigma + j\omega$, where σ is a real number and ω is the real frequency.

For electromagnetic waves in the complex frequency domain for a metallic cylinder, the general solution of wave equations in the complex frequency domain as the cylindrical coordinate can be expressed as,

$$H_z(r, \theta) = (CI_n(s_0 r) + DK_n(s_0 r))\left(Ae^{jn\theta} + Be^{-jn\theta}\right) \tag{5}$$

where r is the distance of the observation point, θ is the observation angle, $s_0 := s\sqrt{\varepsilon_0 \mu_0}$, $I_n(\cdot)$ refers to the modified Bessel functions of the first kind, $K_n(\cdot)$ denotes the modified Bessel functions of the second kind, and A, B, C, and D are unknown coefficients. All the fields can be expanded in terms of the cylindrical vector wave functions, which satisfy Eq. (5), as given below:

$$\mathbf{M}_n(sr, \theta) = \nabla \times \boldsymbol{a}_z Z_n(sr) e^{jn\theta} \tag{6a}$$

$$\mathbf{N}_n(sr, \theta) = \frac{1}{s} \nabla \times \mathbf{M}_n(sr, \theta) \tag{6b}$$

$$\mathbf{L}_n(sr, \theta) = \nabla Z_n(sr) e^{jn\theta} \tag{6c}$$

where $Z_n(\cdot)$ represents the modified Bessel functions. For the incident fields and the field inside a cylinder, $I_n(\cdot)$ is used; for the scatter field, $K_n(\cdot)$ is used.

For the magnetic fields, the scattered outgoing wave $\mathbf{H}^{(s)}$ and the internal wave inside the cylinder $\mathbf{H}^{(T)}$ can be

expanded to an infinite series using Eq. (6b). The equations for these waves are given below.

$$\mathbf{H}^{(i)}(s) = \frac{H_0(s)}{s_0} \sum_{n=-\infty}^{\infty} \mathbf{N}_n(s_0 r, \theta_i - \theta) \tag{7a}$$

$$\mathbf{H}^{(s)}(s) = \frac{H_0(s)}{s_0} \sum_{n=-\infty}^{\infty} A_n \mathbf{N}_n(s_0 r, \theta_i - \theta) \tag{7b}$$

$$\mathbf{H}^{(T)}(s) = \frac{H_0(s)}{s_0} \sum_{n=-\infty}^{\infty} B_n \mathbf{N}_n(s_T r, \theta_i - \theta) \tag{7c}$$

where $H_0(s)$ is expressed as the waveform of the incident wave in the complex frequency domain, A_n is the coefficient of the scattering wave, B_n is the coefficient of the internal wave, and $s_T := s_0\sqrt{\varepsilon_T \mu_r}$, ε_T is the transverse dielectric function.

The electric field can be derived from Maxwell's equations. The internal electric fields of a cylinder are divided into transverse field $\mathbf{E}^{(T)}$ and longitudinal field $\mathbf{E}^{(L)}$, as follows.

$$\mathbf{E}^{(i)}(s) = \frac{(-1)H_0(s)}{s_0} \sum_{n=-\infty}^{\infty} \mathbf{M}_n(s_0 r, \theta_i - \theta) \tag{8a}$$

$$\mathbf{E}^{(s)}(s) = \frac{(-1)H_0(s)}{s_0} \sum_{n=-\infty}^{\infty} A_n \mathbf{M}_n(s_0 r, \theta_i - \theta) \tag{8b}$$

$$\mathbf{E}^{(T)}(s) = \frac{(-1)H_0(s)}{s_T} \sum_{n=-\infty}^{\infty} B_n \mathbf{M}_n(s_T r, \theta_i - \theta) \tag{8c}$$

$$\mathbf{E}^{(L)}(s) = \frac{(-1)H_0(s)}{s_0} \sum_{n=-\infty}^{\infty} G_n \mathbf{L}_n(s_L r, \theta_i - \theta) \tag{8d}$$

where ε_L is the longitudinal dielectric function, $s_L := s_0\sqrt{\varepsilon_L \mu_r}$, and $\mathbf{E}^{(s)}$ is the scattered electric field.

As the boundary condition for the general homogeneous media, the tangential component of the electromagnetic fields is continuous on the boundary. In addition, the boundary condition for a hydrodynamic model can be modified as follows:

$$H_z^{(i)} + H_z^{(s)} = H_z^{(T)} \tag{9a}$$

$$E_\theta^{(i)} + E_\theta^{(s)} = E_\theta^{(T)} + E_\theta^{(L)} \tag{9b}$$

$$E_r^{(i)} + E_r^{(s)} = E_r^{(T)} + E_r^{(L)} \tag{9c}$$

The unknown coefficients can be obtained by solving the linear equations as follows:

$$A_n = -\frac{\begin{matrix} C_n I_n(s_0 a) + I_n(s_0 a) I_n'(s_T a) \\ -\sqrt{\varepsilon_T} I_n'(s_0 a) I_n(s_T a) \end{matrix}}{\begin{matrix} C_n K_n(s_0 a) + K_n(s_0 a) I_n'(s_T a) \\ -\sqrt{\varepsilon_T} K_n'(s_0 a) I_n(s_T a) \end{matrix}} \tag{10a}$$

$$C_n = \frac{n^2}{s_L a} \frac{I_n(s_L a)}{I_n'(s_L a)} I_n(s_T a) \times \left(\frac{\sqrt{\varepsilon_T}}{s_0 a} - \frac{1}{s_T a} \right) \tag{10b}$$

$$B_n = \frac{I_n(s_0 a) + A_n K_n(s_0 a)}{\sqrt{\varepsilon_T} I_n(s_T a)} \tag{10c}$$

$$G_n = -\frac{n}{j s_L s_T a} \times \frac{s_T I_n(s_0 a) + s_T A_n K_n(s_0 a) - s_0 B_n I_n(s_T a)}{I_n'(s_T a)} \tag{10d}$$

To consider the permittivity dispersion $\varepsilon(s)$ for a metal, the relative permittivity of the medium is expressed by the Drude model in the complex frequency domain. In addition, because of the pressure from the electron response, we consider the hydrodynamic model for nonlocal effects. The dielectric function can be divided into transverse and longitudinal dielectric functions. In the hydrodynamic Drude model, the transverse dielectric function ε_T is the same as that in the general Drude model [18], and is represented as,

$$\varepsilon_T(s) = 1 + \frac{f_0 \omega_p^2}{s^2 + \Gamma_0 s} \tag{11}$$

where ω_p is the plasma frequency, f_0 denotes strength, and Γ_0 represents the damping coefficient.

The longitudinal dielectric function ε_L depends not only on frequency but also on the wave number s_0, as follows:

$$\varepsilon_L(s_0, s) = \frac{\omega_p^2}{s^2 + s\Gamma_0 + \beta s_0^2} \tag{12}$$

where $\beta = (3/5)\, v_F^2$ and v_F is the Fermi velocity.

Here, when the medium is not represented by the hydrodynamic Drude model, the coefficients C_n and G_n are zero. In addition, the coefficients for a perfect electric conducting cylinder, dielectric cylinder, and metallic nanosphere are provided in the appendix.

III. REFERENCE SOLUTIONS

To validate our solutions, we refer to the scattered electromagnetic waves for the metallic cylinder. The radius of the cylinder is $a = 1.0$ nm. The incident wave is a plane wave, which originates from $\theta_i = 180°$. Further, the medium is gold and we use the hydrodynamic Drude model [16]. The incident waveform is a modulated Gaussian pulse, which is generally used in time domain solvers. Because the Laplace transform of the Gaussian type of pulses cannot be defined, we derived the pseudo-Gaussian pulse [19]. The center wavelength of the modulated Gaussian pulse is 444 nm, which is the plasmon resonance wavelength.

Here, to consider the standard FDTD method for comparison, the modeling for the scatterer uses the staircase approximation and the second-order accurate central-difference scheme is applied. The cell size Δx $(= \Delta y)$ for the FDTD method is 0.1 nm, which is one-tenth of the cylinder radius. The time increment Δt of an explicit FDTD method is restricted by the maximum time step size Δt_{CFL}, which is satisfied the Courant–Friedrichs–Lewy (CFL) condition based on a cell size, for stable calculation. The observation time in the FDTD method tends to be a random number. Fig. 3 (a) and (b) show the electric field distributions obtained by our reference solution and the FDTD method, respectively, at $t = 22.48670284948268$ fs. Here, the observation time

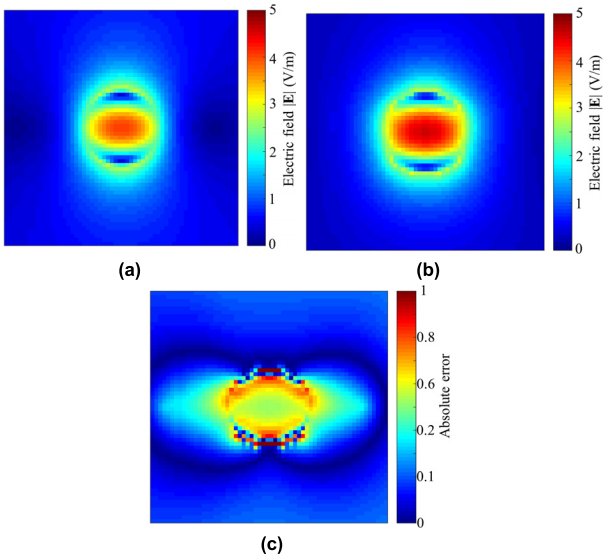

FIGURE 3. Electric field distribution for metallic nanocylinder at t = 22.48670284948268 fs. (a) Our solution, (b) FDTD result, and (c) Absolute error between our solutions and the FDTD result. The field distribution at a specific observation time can be evaluated using our reference solution.

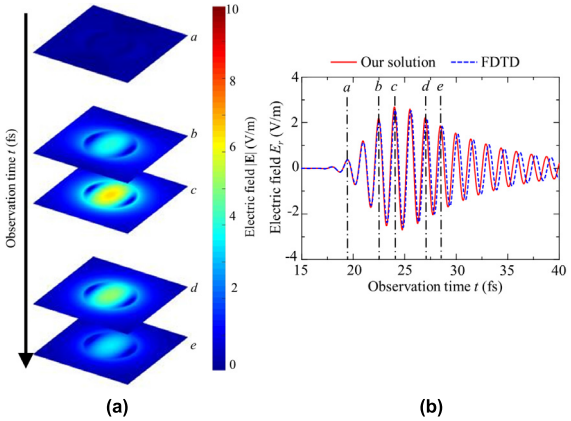

FIGURE 4. Our solutions for arbitrary observation time. (a) Electric field distribution for arbitrary observation time, and (b) Time domain response. By certainly focusing on an observation point and discretely changing the observation time, the time response of the electromagnetic field can be obtained.

is determined by the time step size $\Delta t = 0.99 \times \Delta t_{\mathrm{CFL}}$. The absolute error between these two methods is shown in Fig. 3(c). It is clear that only our solution can accurately evaluate the field distribution at a desired observation time.

Fig. 4(a) and (b) show the field distributions for the arbitrary observation time and the time domain response of the electric field for the r-component at the observation point, which is $(r, \theta) = (1.2\ \mathrm{nm}, 90°)$, respectively. Our solution for field distribution can arbitrarily select a specific observation time. By certainly focusing on an observation point and changing the observation time discretely, the time response of the electromagnetic field can be obtained. In this case, for a pulse including a plasmon resonance wavelength, the difference between both results increases with the observation time.

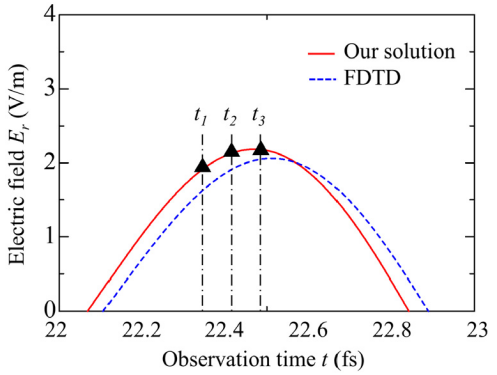

FIGURE 5. Time responses of the FDTD method are evaluated at a specific observation time. Our results can select an arbitrary observation time.

TABLE 1. Truncation number of FILT k required for 7 digits of accuracy. Our method can determine the observation time and the sampling complex frequency.

Observation time t (fs)	Truncation number of FILT k	Electric field E_r (Our solutions)	Electric field E_r (FDTD)
22.34659878188465	49	1.9218211	1.6979585
22.41665081568366	49	2.1364631	1.9529556
22.48670284948268	49	2.1814205	2.0589861

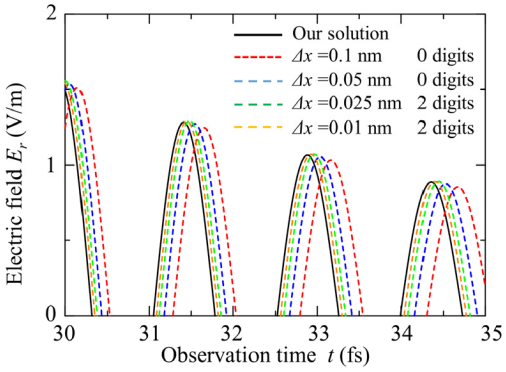

FIGURE 6. Computational accuracy of the FDTD method for various cell sizes. The FDTD results converge to our results as the cell size reduces.

Here, the time domain response obtained by the FDTD method is evaluated using our solutions. Fig. 5 shows that the time domain response of the FDTD method is estimated at a specific observation time. The time step size of the FDTD method is $2.335067793300381 \times 10^{-19}$ s, which satisfies the stable condition for an explicit method. In our reference, the solution can be selected using an arbitrary observation time, which is useful for evaluating the time domain response. Table 1 shows the truncation number of FILT k required for converging to seven digits of accuracy. Here, we confirm the convergence history for varying the truncation number of FILT. In our method, the sampling frequency for inverse Laplace transform can be determined by using our algorithm.

To confirm the computational accuracy of the FDTD method, a convergence test is conducted by varying the cell size. Fig. 6 shows the time domain response for various cell sizes. The difference between our result and the FDTD results appears in the phase rather than the amplitude, when the cell size is coarse. On the other hand, the amplitude is determined by the charge distribution based on nonlocal effects. The FDTD results converge to our results with the reduction in cell size. The number of digits of agreement is 2 when the cell size is 0.025 nm.

IV. CONCLUSION

An evaluation method for time domain electromagnetic solver was proposed in this study. The reference solutions of electromagnetic waves in the time domain for a nanocylinder with nonlocal effects were derived. The solutions for a metallic nanocylinder were modeled using the hydrodynamic Drude model and defined in the complex frequency domain. These solutions were then transformed into the time domain by FILT. The time domain response for a perfect electric conducting cylinder, dielectric cylinder, and metallic nanosphere is shown in the appendix. Using our highly reliable time domain response at a specific observation time, the numerical accuracy for the time domain methods was evaluated. The original data will be provided online (DOI:10.21227/dj4j-3647). These solutions can be applied for further developing time domain solvers.

APPENDIX

The purpose of our solution is to verify a wide variety of time domain solvers, such as verifying the accuracy of FDTD codes created by students and proof of concept for novel computational techniques. The coefficients and samples of reference solution for the scattering problems discussed in textbooks are described here; for example, scattering from a perfect conducting cylinder, dielectric cylinder, and metallic nanosphere. The original data will be provided online.

A. SOLUTION FOR A PERFECT ELECTRIC CONDUCTING CYLINDER

For a perfectly conducting cylinder, the following boundary condition applies: the tangential component of the electric field vanishes at the boundary. The unknown coefficient can be determined as follows:

$$A_n = -\frac{I_n'(s_0 a)}{K_n'(s_0 a)} \tag{A1}$$

$$B_n = C_n = G_n = 0 \tag{A2}$$

Fig. 7 shows the electric field distribution at $t = 1.27000000000000$ fs; Fig. 8 shows the time domain response of the electric field. The radius a of the cylinder is 100 nm, and the incident wave is assumed to be a plane wave. The waveform is a pseudo-Gaussian pulse [19], whose parameters of image function are $M = 36$ and $\Omega_g = 1 \times 10^{-16}$. The incident angle θ_i is 180°. The coordinates of the observation point (r, θ) are (200 nm, 180°).

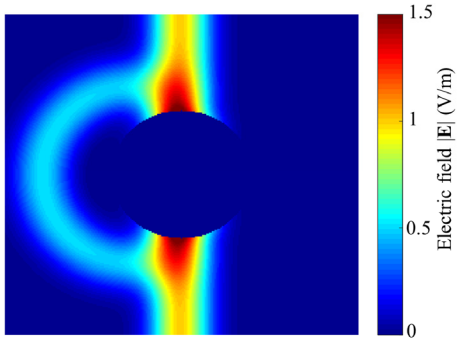

FIGURE 7. Electric field distribution for a perfectly conducting cylinder at $t = 1.27000000000000$ fs.

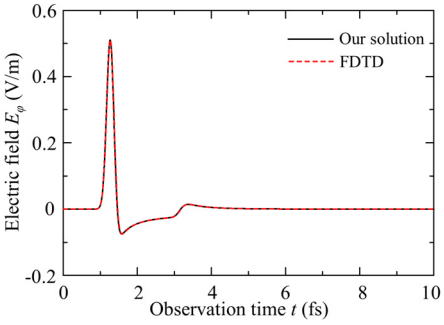

FIGURE 8. Time domain response for a perfectly conducting cylinder.

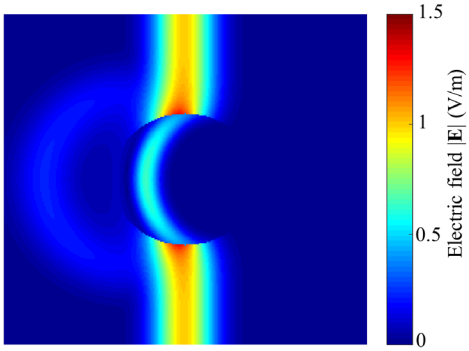

FIGURE 9. Electric field distribution for a dielectric conducting cylinder at $t = 1.27000000000000$ fs.

B. SOLUTION FOR A DIELECTRIC CYLINDER

For a dielectric cylinder, the boundary condition is such that the tangential component of the electromagnetic field is continuous on the surface. The unknown coefficient can be determined using the following equations:

$$A_n = -\frac{I_n(s_0 a)\, I_n'(s_1 a) - \sqrt{\varepsilon}_r I_n'(s_0 a)\, I_n(s_1 a)}{K_n(s_0 a)\, I_n'(s_1 a) - \sqrt{\varepsilon}_r K_n'(s_0 a)\, I_n(s_1 a)} \tag{A3}$$

$$B_n = \frac{I_n(s_0 a) + A_n K_n(s_0 a)}{\sqrt{\varepsilon}_r I_n'(s_1 a)} \tag{A4}$$

$$C_n = G_n = 0 \tag{A5}$$

Fig. 9 shows the electric field distribution at $t = 1.27000000000000$ fs; Fig. 10 shows the time domain

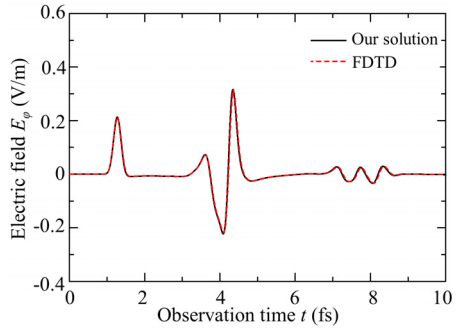

FIGURE 10. Time domain response for a dielectric cylinder.

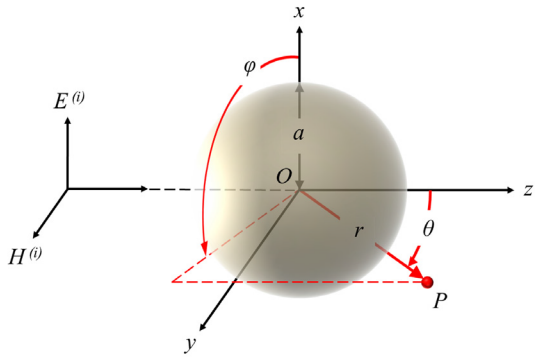

FIGURE 11. Geometry and coordinate system of the sphere. The scatterer consists of metal with permittivity $\varepsilon(s)$ and radius a. $\mathbf{E^{(i)}}$ and $\mathbf{H^{(i)}}$: incident waves, θ_i: angle of incidence.

response of the electric field. The radius a and relative permittivity of the cylinder are 100 nm and 5, respectively. The incident wave is assumed to be a plane wave. The waveform is a pseudo-Gaussian pulse, whose parameters of the image function are $M = 36$ and $\Omega_g = 1 \times 10^{-16}$. The incident angle θ_i is 180°; the coordinates of the observation point (r, θ) are (200 nm, 180°).

C. SOLUTION FOR A METALLIC NANOSPHERE WITH NONLOCAL EFFECTS IN THE COMPLEX FREQUENCY DOMAIN

Fig. 11 shows the geometry and coordinate systems. The scattering electric field for a metallic nanosphere with nonlocal effects can be derived as,

$$E^{(s)}(P) = -E_0(s)e^{st} \times \sum_{n=-\infty}^{\infty} j^{-n} \frac{2n+1}{n(n+1)} \left(b_n \mathbf{M_{1n}}(P) - jc_n \mathbf{N_{1n}}(P)\right) \tag{A6}$$

where

$$\mathbf{M_{mn}} = \nabla \times \left[\hat{\boldsymbol{a}}_{\boldsymbol{r}} \psi\,(r, \theta, \varphi)\right] \tag{A7a}$$

$$\mathbf{N_{mn}} = \frac{1}{S} \nabla \times \mathbf{M_{mn}} \tag{A7b}$$

$$\psi\,(r, \theta, \varphi) = z_n\,(sr)\, P_n^m(\cos\theta) e^{jm\varphi} \tag{A7c}$$

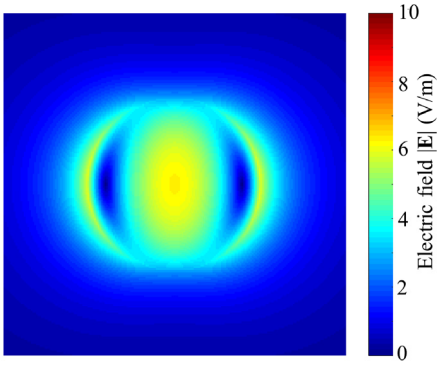

FIGURE 12. Electric field distribution at $t = 26.8900000000000$ fs on the x–y plane. The field of hydrodynamic Drude model is distributed not only along the side but also within the sphere.

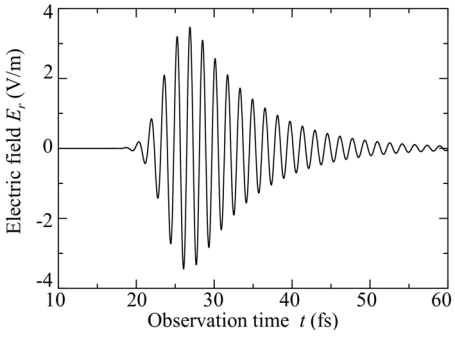

FIGURE 13. Time domain response for the metallic nanosphere. Because the resonance frequency is included in the incident pulse, a long time is taken for the energy stored inside the sphere to be released.

where $z_n(\cdot)$ represents the modified spherical Bessel functions and $P_n^m(\cdot)$ represents the associated Legendre polynomials. The unknown scattering coefficients can be obtained using the boundary conditions as follows:

$$b_n = -\frac{\begin{matrix} I_n\,(s_T a)\,(s_0 a I_n\,(s_0 a))' \\ -I_n\,(s_0 a)\,(s_T a I_n\,(s_T a))' \end{matrix}}{\begin{matrix} I_n\,(s_T a)\,(s_0 a K_n\,(s_0 a))' \\ -K_n\,(s_0 a)\,(s_0 a I_n\,(s_T a))' \end{matrix}} \tag{A8a}$$

$$c_n = -\frac{\begin{matrix} CI_n\,(s_0 a) \\ +I_n'\,(s_L a) \left\{ \begin{matrix} I_n\,(s_0 a)\,(s_T a I_n\,(s_T a))' \\ -\sqrt{\varepsilon_T} I_n\,(s_T a)\,(s_0 a I_n\,(s_0 a))' \end{matrix} \right\} \end{matrix}}{\begin{matrix} CK_n\,(s_0 a) \\ +I_n'\,(s_L a) \left\{ \begin{matrix} K_n\,(s_0 a)\,(s_T a I_n\,(s_T a))' \\ -\sqrt{\varepsilon_T} I_n\,(s_T a)\,(s_0 a K_n\,(s_0 a))' \end{matrix} \right\} \end{matrix}} \tag{A8b}$$

$$C = n\,(n+1)\,\frac{I_n\,(s_L a)}{I_n'\,(s_L a)} I_n\,(s_T a)\left(\sqrt{\varepsilon_T} - 1\right) \tag{A8c}$$

Here, when the medium is not represented by the hydrodynamic Drude model, the coefficient C is equal to zero.

Fig. 12 shows the electric field distribution at $t = 26.8900000000000$ fs on the x–y plane and $z = 0$; Fig. 13 shows the time response. The field is distributed not only along the side but also within the sphere. The parameters

of the modified Gaussian pulse incidence are $M = 64$, $\omega_m = 2\pi \times 482 \times 10^{-9}$, and $\Omega_g = 1.919144741316492 \times 10^{-15}$. The electric fields increase with time. Because the resonance frequency is included in the incident pulse, releasing of the energy stored inside the sphere requires a long time.

ACKNOWLEDGMENT

The authors would like to thank Prof. J. Yamauchi and Prof. J. Shibayama, Hosei University, and S. Watanabe, Mitsubishi Electric Corporation, for their helpful discussion in this study.

REFERENCES

[1] H. Zheng, Y. Wu, K. Zhang, L. Wang, M. Wang, and E. Li, "Wide-band modeling on-chip spiral inductors using frequency-dependent conformal ADI-FDTD method," *IEEE Access*, vol. 7, pp. 184940–184949, 2019.
[2] W. Tang, C. Argyropoulos, E. Kallos, W. Song, and Y. Hao, "Discrete coordinate transformation for designing all-dielectric flat antennas," *IEEE Trans. Antennas Propag.*, vol. 58, no. 12, pp. 3795–3804, Dec. 2010.
[3] M. Cavagnaro, C. Amabile, P. Bernardi, S. Pisa, and N. Tosoratti, "A minimally invasive antenna for microwave ablation therapies: Design, performances, and experimental assessment," *IEEE Trans. Biomed. Eng.*, vol. 58, no. 4, pp. 949–959, Apr. 2011.
[4] V. Nayyeri, M. Soleimani, and O. M. Ramahi, "Modeling graphene in the finite-difference time-domain method using a surface boundary condition," *IEEE Trans. Antennas Propag.*, vol. 61, no. 8, pp. 4176–4182, Aug. 2013.
[5] A. Taflove, A. Oskooi, and S. G. Johnson, *Advances in FDTD Computational Electrodynamics: Photonics and Nanotechnology*. Norwood, MA, USA: Artech House, 2013.
[6] J. Liu, M. Brio, Y. Zeng, A. R. Zakharian, W. Hoyer, S. W. Koch, and J. V. Moloney, "Generalization of the FDTD algorithm for simulations of hydrodynamic nonlinear Drude model," *J. Comput. Phys.*, vol. 229, no. 17, pp. 5921–5932, Aug. 2010.
[7] S. Ohnuki, T. Kato, Y. Takano, Y. Ashizawa, and K. Nakagawa, "Design and numerical verification of plasmonic cross antennas to generate localized circularly polarized light for all-optical magnetic recording," *Radio Sci.*, vol. 50, no. 1, pp. 29–40, Jan. 2015.
[8] P. Li, L. J. Jiang, and H. Bagci, "Discontinuous Galerkin time-domain modeling of graphene nanoribbon incorporating the spatial dispersion effects," *IEEE Trans. Antennas Propag.*, vol. 66, no. 7, pp. 3590–3598, Jul. 2018.
[9] I. Bisio, M. Cerruti, F. Lavagetto, M. Marchese, M. Pastorino, A. Randazzo, and A. Sciarrone, "A trainingless WiFi fingerprint positioning approach over mobile devices," *IEEE Antennas Wireless Propag. Lett.*, vol. 13, pp. 832–835, 2014.
[10] E. Lucano, M. Liberti, G. G. Mendoza, T. Lloyd, M. I. Iacono, F. Apollonio, S. Wedan, W. Kainz, and L. M. Angelone, "Assessing the electromagnetic fields generated by a radiofrequency MRI body coil at 64 MHz: Defeaturing versus accuracy," *IEEE Trans. Biomed. Eng.*, vol. 63, no. 8, pp. 1591–1601, Aug. 2016.
[11] J. J. Bowman, T. B. A. Senior, and P. L. E. Uslenghi, *Electromagnetic and Acoustic Scattering by Simple Shapes*. Amsterdam, The Netherlands: North Holland, 1969.
[12] A. Taflove and S. C. Hagness, *Computational Electrodynamics: The Finite-Difference Time-Domain Method*. Norwood, MA, USA: Artech House, 2005.
[13] A. Taflove and S. C. Hagness, *Computational Electrodynamics*, 2nd ed. Norwood, MA, USA: Artech House, 1995.
[14] T. Hosono, "Numerical inversion of laplace transform and some applications to wave optics," *Radio Sci.*, vol. 16, no. 6, pp. 1015–1019, 1981.
[15] S. Ohnuki, R. Ohnishi, D. Wu, and T. Yamaguchi, "Time-division parallel FDTD algorithm," *IEEE Photon. Technol. Lett.*, vol. 30, no. 24, pp. 2143–2146, Dec. 15, 2018.
[16] Y. Luo, A. I. Fernandez-Dominguez, A. Wiener, S. A. Maier, and J. B. Pendry, "Surface plasmons and nonlocality: A simple model," *Phys. Rev. Lett.*, vol. 111, pp. 093901-1–093901-5, Aug. 2013.
[17] R. Ruppin, "Extinction properties of thin metallic nanowires," *Opt. Commun.*, vol. 190, nos. 1–6, pp. 205–209, Apr. 2001.
[18] A. D. Rakić, A. B. Djurišić, J. M. Elazar, and M. L. Majewski, "Optical properties of metallic films for vertical-cavity optoelectronic devices," *Appl. Opt.*, vol. 37, no. 22, p. 5271, Aug. 1998.
[19] D. Wu, R. Ohnishi, R. Uemura, T. Yamaguchi, and S. Ohnuki, "Finite-difference Complex-Frequency-Domain method for optical and plasmonic analyses," *IEEE Photon. Technol. Lett.*, vol. 30, no. 11, pp. 1024–1027, Jun. 1, 2018.

SOICHIRO MASUDA was born in Chiba, Japan, in 1996. He received the B.S. degree in electrical engineering from Nihon University, Tokyo, Japan, in 2018, where he is currently pursuing the master's degree. His research interest includes electromagnetic scattering.

SEIYA KISHIMOTO was born in Chiba, Japan, in 1987. He received the B.S., M.S., and Ph.D. degrees in electrical engineering from Nihon University, Tokyo, Japan, in 2009, 2011, and 2014, respectively. From 2014 to 2019, he was a Research Scientist with the Wireless System Laboratory, Research and Development Center, Toshiba Corporation. In 2019, he joined the Department of Electrical Engineering, College of Science and Technology, Nihon University, where he currently holds an assistant position. His research interests include small antennas, tunable antennas, RFID, and fast solvers. He was a Research Fellow of the Japan Society for the Promotion of Science (JSPS), in 2013.

SHINICHIRO OHNUKI (Member, IEEE) was born in Tokyo, Japan, in 1968. He received the B.S., M.S., and Ph.D. degrees in electrical engineering from Nihon University, Tokyo, in 1991, 1993, and 2000, respectively.

From 2000 to 2004, he was with the Center for Computational Electromagnetics and the Electromagnetics Laboratory, Department of Electrical and Computer Engineering, as a Postdoctoral Research Associate and a Visiting Lecturer, and later as a Visiting Associate Professor, in 2012. He joined the Department of Electrical Engineering, College of Science and Technology, Nihon University, in 2004, where he is currently a Professor. His research interests include computational electromagnetics and multiphysics simulation. He was a recipient of the Research Fellowship Award from the Kajima Foundation, Tokyo, in 2000. He was a co-recipient of the Best Paper Award from the Magnetic Society of Japan, in 2013, and the Technical Development Award from the Institute of Electrical Engineers of Japan, in 2014. He has been an Editorial Board Member of the *Progress in Electromagnetics Research*, since 2017, a Guest Editor of *Radio Science*, since 2019, and the Secretary of the URSI Committee, Japan, and URSI Commission B, since 2017. He was an Associate Editor of the *Applied Computational Electromagnetics Society Express Journal*, in 2016. He has been an Associate Editor of the IEEE JOURNAL ON MULTISCALE AND MULTIPHYSICS COMPUTATIONAL TECHNIQUES, since 2018.